Supporting information for

# Multifunctional chiral metal hydrogen-bonded organic frameworks constructed from lanthanide ions with trigonal prismatic coordination environment

Guo Peng,*[a] Guo-Xing Zhou, [a] Xiang-Tao Dong, [a] Yong-Bo Peng, [a] Rong-Yan Zhang,[a] Ying-Zhao Ma,[b] and Xiao-Ming Ren*[ac]

[a] State Key Laboratory of Materials-Oriented Chemical Engineering, School of Chemistry and Molecular Engineering, Nanjing Tech University, Nanjing 211816, P. R. China

[b] Chongqing Key Laboratory of Green Synthesis and Application, College of Chemistry, Chongqing Normal University, Chongqing 401331, China

[c] State Key Laboratory of Coordination Chemistry, Nanjing University, Nanjing 210093, P. R. China

E-mail: guopeng@njtech.edu.cn, xmren@njtech.edu.cn

**Table S1** Crystallographic data and structure refinement for complexes **D-1**, **L-1**, **D-2** and **L-2**.

| | **D-1** | **L-1** | **D-2** | **L-2** |
|---|---|---|---|---|
| Formula | $C_{18}H_{37}DyN_3O_{17}P_3$ | $C_{18}H_{37}DyN_3O_{17}P_3$ | $C_{18}H_{37}N_3O_{17}P_3Yb$ | $C_{18}H_{37}N_3O_{17}P_3Yb$ |
| $M_r$ (g mol$^{-1}$) | 822.91 | 822.91 | 833.45 | 833.45 |
| Crystal system | Tetragonal | Tetragonal | Tetragonal | Tetragonal |
| Space group | $P4_3$ | $P4_1$ | $P4_3$ | $P4_1$ |
| $T$ (K) | 296 | 296 | 296 | 296 |
| $a$ (Å) | 12.4345(3) | 12.4378(3) | 12.4178(7) | 12.4055(9) |
| $b$ (Å) | 12.4345(3) | 12.4378(3) | 12.4178(7) | 12.4055(9) |
| $c$ (Å) | 18.7179(11) | 18.7219(10) | 18.6104(11) | 18.6422(14) |

| | | | | |
|---|---|---|---|---|
| $\alpha$ (°) | 90 | 90 | 90 | 90 |
| $\beta$ (°) | 90 | 90 | 90 | 90 |
| $\gamma$ (°) | 90 | 90 | 90 | 90 |
| $V$ (Å$^3$) | 2894.1(2) | 2896.3(2) | 2869.8(4) | 2869.0(3) |
| $Z$ | 4 | 4 | 4 | 4 |
| $D_c$ (g cm$^{-3}$) | 1.889 | 1.887 | 1.927 | 1.930 |
| $\mu$ (mm$^{-1}$) | 2.829 | 2.827 | 3.508 | 3.509 |
| $F$(000) | 1652 | 1652 | 1664 | 1668 |
| Reflns collected | 19262 | 30796 | 16775 | 15861 |
| Unique reflns | 4953 | 9243 | 4931 | 4768 |
| $R_{int}$ | 0.0559 | 0.0619 | 0.0579 | 0.0226 |
| GOF | 1.042 | 1.055 | 1.022 | 1.325 |
| $R_1$(I > 2σ) | 0.0250 | 0.0356 | 0.0250 | 0.0221 |
| w$R_2$ (all data) | 0.0612 | 0.0754 | 0.0572 | 0.0813 |
| Max. diff. peak / hole (e Å$^{-3}$) | 1.068/-0.671 | 2.101/ -1.424 | 0.858/-0.575 | 1.974/-0.965 |
| Flack parameter | 0.075(11) | 0.040(9) | 0.074(10) | -0.008(3) |

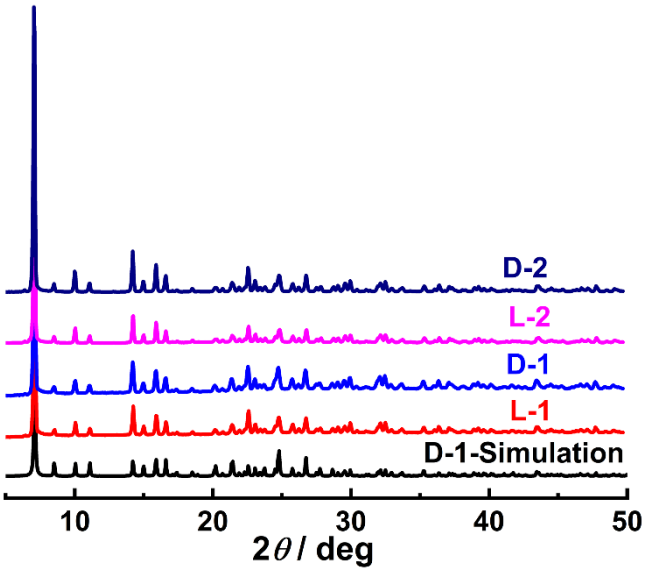


**Fig. S1** Measured and simulated PXRD patterns of complexes **D-1**, **L-1**, **D-2** and **L-2**.

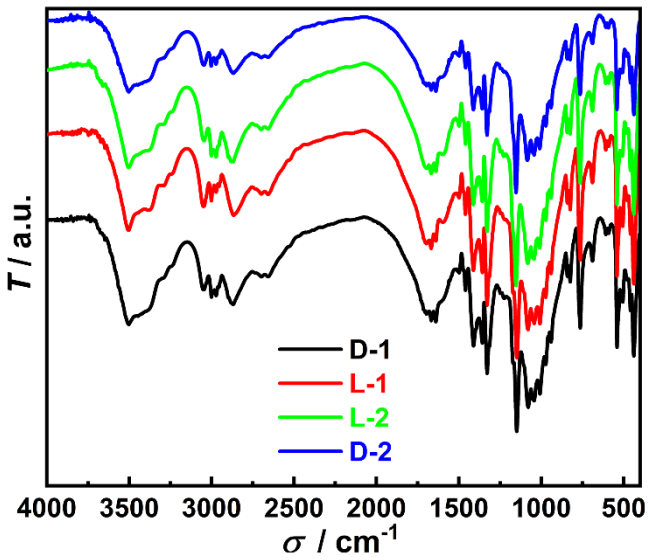


**Fig. S2** IR spectra of complexes **D-1**, **L-1**, **D-2** and **L-2**.

**Table S2** Continuous shape measures (CShM) for complex **D-1**.

| | **D-1** |
|---|---|
| HP-6 | 32.793 |
| PPY-6 | 18.607 |
| OC-6 | 5.086 |
| **TPR-6** | **3.931** |
| JPPY-6 | 22.568 |

HP-6 = Hexagon, PPY-6 = Pentagonal pyramid, OC-6 = Octahedron, **TPR-6 = Trigonal prism**, JPPY-6 = Johnson pentagonal pyramid J2

**Table S3** Selected bond lengths (Å) and angles (º) for **D-1**.

| **D-1** | |
|---|---|
| Dy(1)-O(1) | 2.267(4) |
| Dy(1)-O(2)#1 | 2.259(4) |
| Dy(1)-O(6) | 2.225(4) |
| Dy(1)-O(7)#2 | 2.253(5) |
| Dy(1)-O(1)#1 | 2.252(4) |
| Dy(1)-O(12)#2 | 2.251(5) |
| O(2)#1-Dy(1)-O(1) | 87.79(16) |
| O(6)-Dy(1)-O(1) | 81.39(16) |
| O(6)-Dy(1)-O(2)#1 | 111.39(17) |
| O(6)-Dy(1)-O(7)#2 | 85.80(17) |
| O(6)-Dy(1)-O(1)#1 | 80.65(16) |
| O(6)-Dy(1)-O(12)#2 | 155.99(17) |

| | |
|---|---|
| O(7)#2-Dy(1)-O(1) | 111.02(18) |
| O(7)#2-Dy(1)-O(2)#1 | 156.70(18) |
| O(1)#1-Dy(1)-O(1) | 154.83(17) |
| O(1)#1-Dy(1)-O(2)#1 | 82.52(17) |
| O(1)#1-Dy(1)-O(7)#2 | 85.07(19) |
| O(12)#2-Dy(1)-O(1) | 82.45(16) |
| O(12)#2-Dy(1)-O(2)#1 | 85.54(18) |
| O(12)#2-Dy(1)-O(7)#2 | 83.56(17) |
| O(12)#2-Dy(1)-O(1)#1 | 119.63(17) |

Symmetry codes: #1 y, 1-x, 0.25+z; #2 1-y, x, -0.25+z.

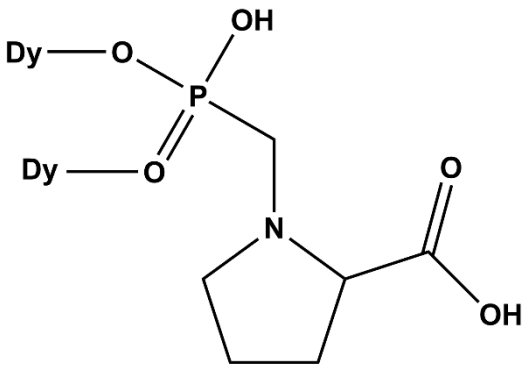


**Scheme S1** The coordination mode of PMP ligand in **D-1**.

**Table S4** Hydrogen bonds in **D-1**.

| D-H···A | d(D-H)/ Å | d(H···A)/ Å | d(D···A)/ Å | <(DHA)/ º |
|---|---|---|---|---|
| N1-H1 ···O14 | 0.98 | 1.80 | 2.707(7) | 153 |
| N2-H2 ···O4 | 0.98 | 1.95 | 2.852(7) | 152 |
| O3-H3 ···O15 | 0.82 | 1.78 | 2.551(7) | 156 |
| N3-H3A ···O9 | 0.98 | 1.87 | 2.774(7) | 151 |
| O8-H8 ···O5 | 0.82 | 1.72 | 2.443(7) | 146 |
| O13-H13 ···O10 | 0.82 | 1.73 | 2.438(7) | 143 |
| O16-H16C ···O17 | 0.85 | 2.07 | 2.871(13) | 156 |
| O16-H16D ···O5 | 0.85 | 2.18 | 2.957(9) | 152 |
| O17-H17A ···O16 | 0.85 | 2.10 | 2.781(13) | 137 |
| O17-H17B ···O10 | 0.85 | 2.45 | 3.005(10) | 123 |
| C1-H1B ···O4 | 0.97 | 2.55 | 3.111(8) | 117 |
| C4-H4B ···O13 | 0.97 | 2.37 | 3.324(9) | 169 |
| C8-H8B ···O7 | 0.97 | 2.59 | 3.147(9) | 117 |
| C11-H11 ···O15 | 0.98 | 2.57 | 3.420(8) | 145 |
| C13-H13B ···O14 | 0.97 | 2.48 | 3.034(8) | 116 |
| C14-H14B ···O12 | 0.97 | 2.55 | 3.016(9) | 109 |

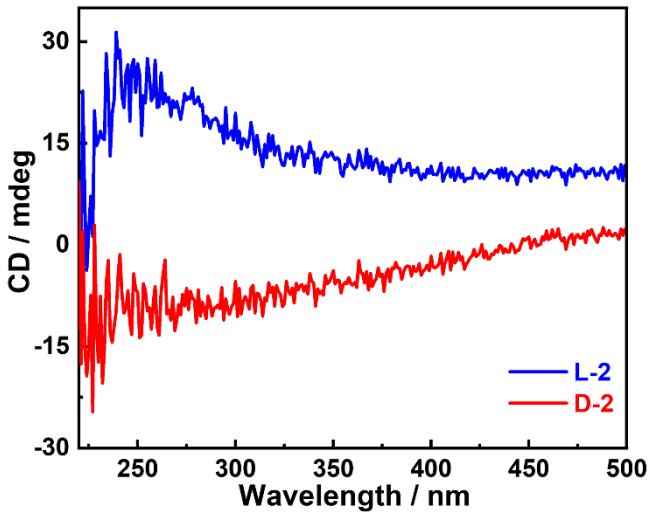


**Fig. S3** CD spectra of complexes **D-2** and **L-2**.

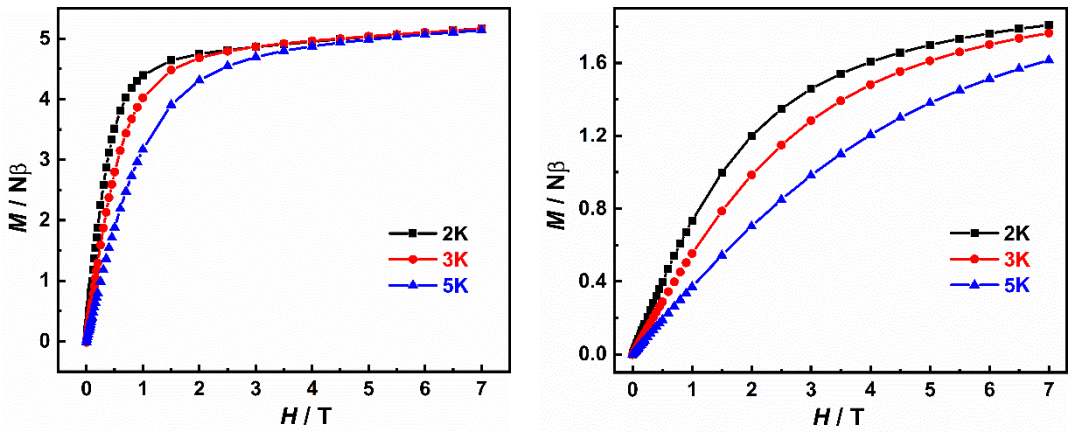


**Fig. S4** *M* vs. *H* plots for **L-1** (left) and **L-2** (right).

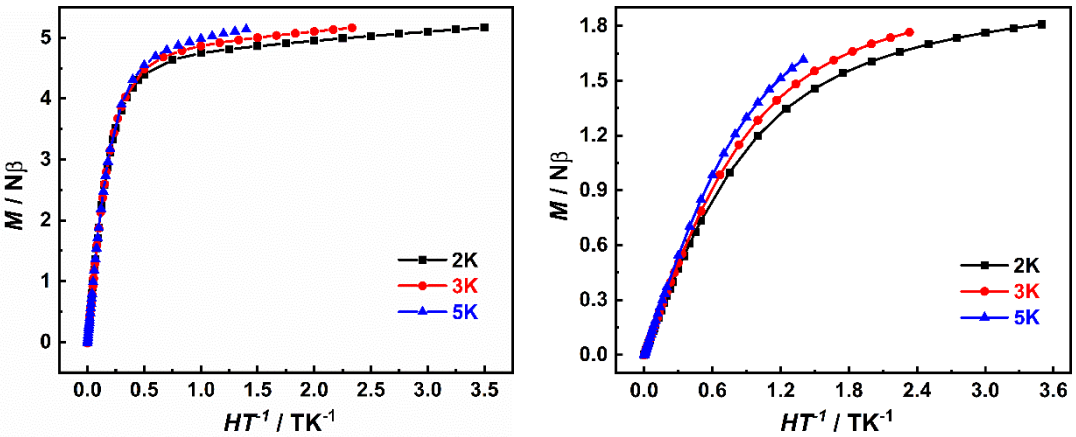


**Fig. S5** *M* vs. $HT^{-1}$ plots for **L-1** (left) and **L-2** (right).

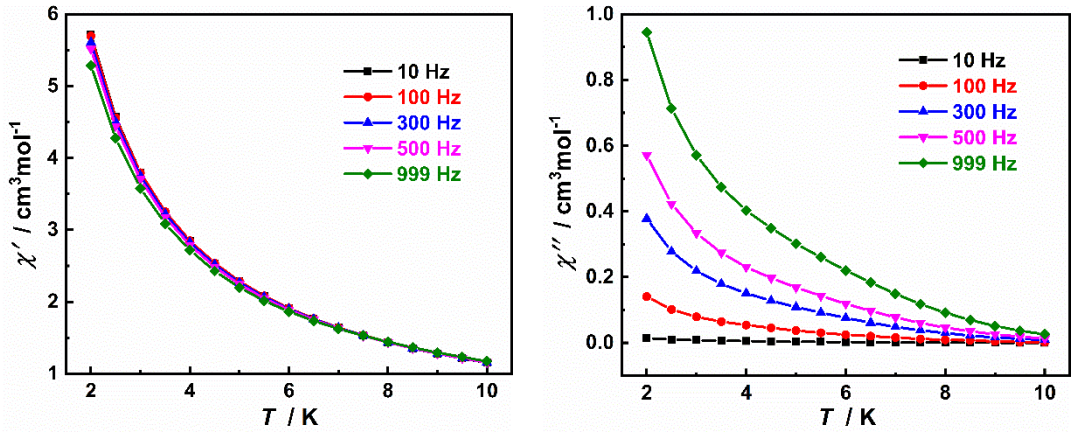


**Fig. S6** Temperature dependence of in-phase (left) and out-of-phase (right) ac susceptibility data at a zero dc field for **L-1**.

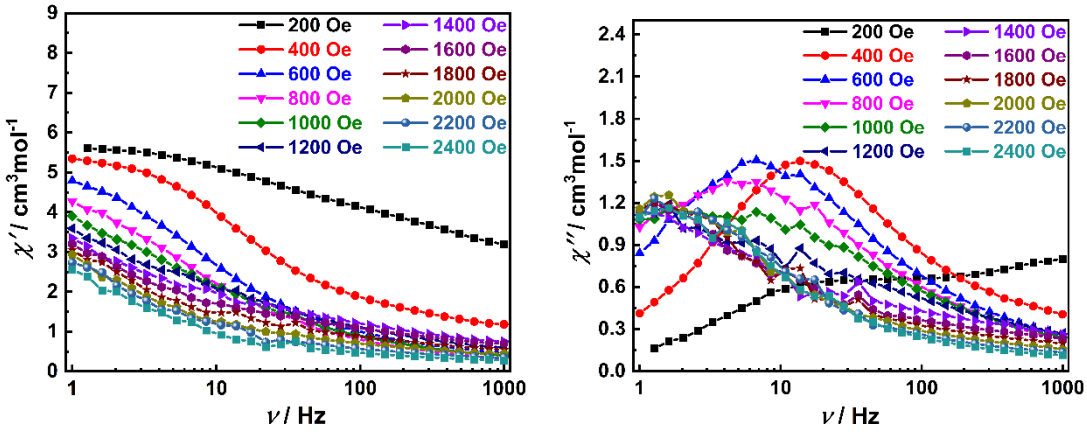


**Fig. S7** Frequency dependence of in-phase (left) and out-of-phase (right) ac susceptibility signals under different dc fields at 2K for **L-1**.

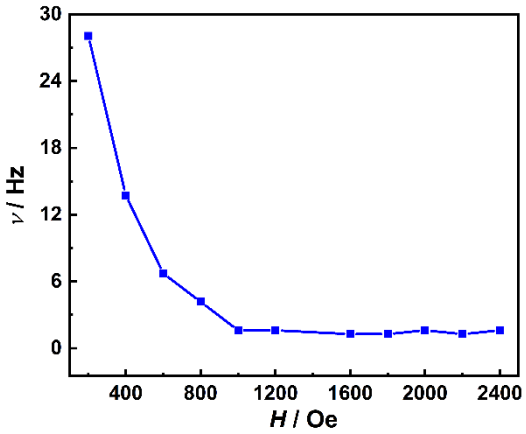


**Fig. S8** Field dependence of the characteristic frequency for **L-1** at 2K.

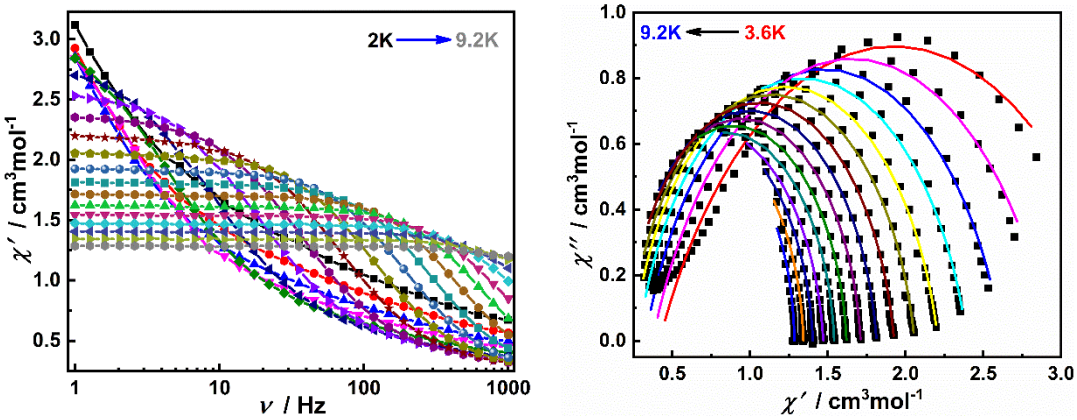


**Fig. S9** Frequency dependence of in-phase (left) ac susceptibility data under a 1600 Oe dc field for **L-1**. Cole–Cole plots for **L-1** (right). The solid lines are the best fits to a generalized Debye model.

**Table S5** Cole-Cole parameters of **L-1** at a 1600 Oe dc field.

| $T$ / K | $\chi_S$ / cm$^{-3}$mol$^{-1}$ | $\chi_T$ / cm$^{-3}$mol$^{-1}$ | $\tau$ / s | $\alpha$ | R |
|---|---|---|---|---|---|
| 3.6 | 4.17E-01 | 3.43E+00 | 3.63E-02 | 3.17E-01 | 1.04E-01 |
| 4 | 3.73E-01 | 2.94E+00 | 1.62E-02 | 2.48E-01 | 5.84E-02 |
| 4.4 | 3.26E-01 | 2.62E+00 | 7.86E-03 | 2.05E-01 | 2.68E-02 |
| 4.8 | 2.79E-01 | 2.40E+00 | 4.07E-03 | 1.76E-01 | 1.22E-02 |
| 5.2 | 2.47E-01 | 2.21E+00 | 2.23E-03 | 1.48E-01 | 6.90E-03 |
| 5.6 | 2.22E-01 | 2.06E+00 | 1.30E-03 | 1.26E-01 | 4.99E-03 |
| 6 | 1.96E-01 | 1.93E+00 | 7.91E-04 | 1.10E-01 | 3.48E-03 |
| 6.4 | 1.85E-01 | 1.81E+00 | 5.08E-04 | 9.36E-02 | 2.55E-03 |
| 6.8 | 1.79E-01 | 1.71E+00 | 3.40E-04 | 7.70E-02 | 2.38E-03 |
| 7.2 | 1.64E-01 | 1.62E+00 | 2.33E-04 | 6.52E-02 | 1.72E-03 |
| 7.6 | 1.46E-01 | 1.54E+00 | 1.63E-04 | 5.83E-02 | 1.50E-03 |
| 8 | 2.89E-02 | 1.47E+00 | 1.07E-04 | 7.61E-02 | 5.56E-03 |
| 8.4 | 1.18E-13 | 1.40E+00 | 7.66E-05 | 5.86E-02 | 8.38E-04 |
| 8.8 | 2.13E-13 | 1.34E+00 | 5.83E-05 | 4.01E-02 | 1.03E-03 |
| 9.2 | 8.01E-13 | 1.28E+00 | 4.59E-05 | 1.80E-02 | 1.33E-03 |

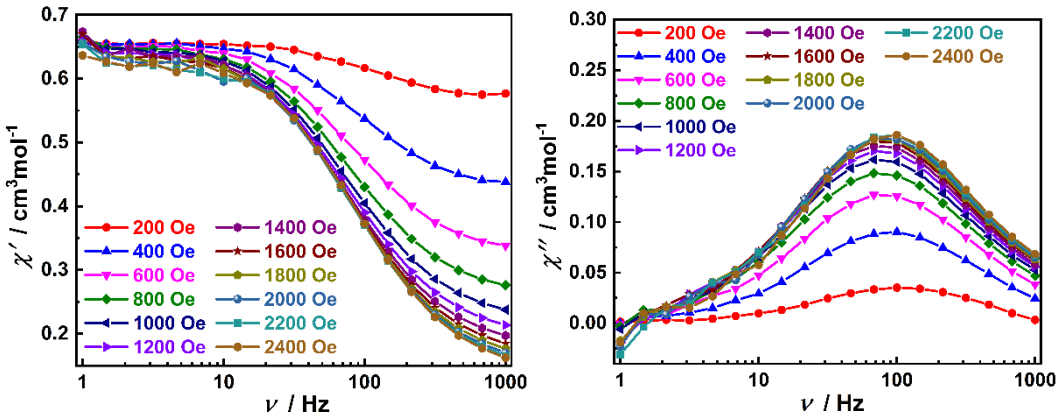


**Fig. S10** Frequency dependence of in-phase (left) and out-of-phase (right) ac susceptibility signals under different dc fields at 2 K for **L-2**.

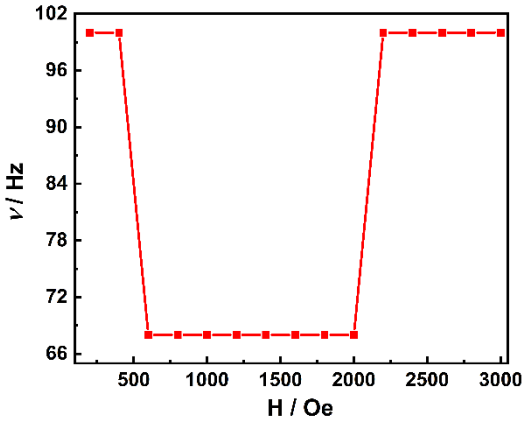


**Fig. S11** Field dependence of the characteristic frequency for **L-2** at 2K.

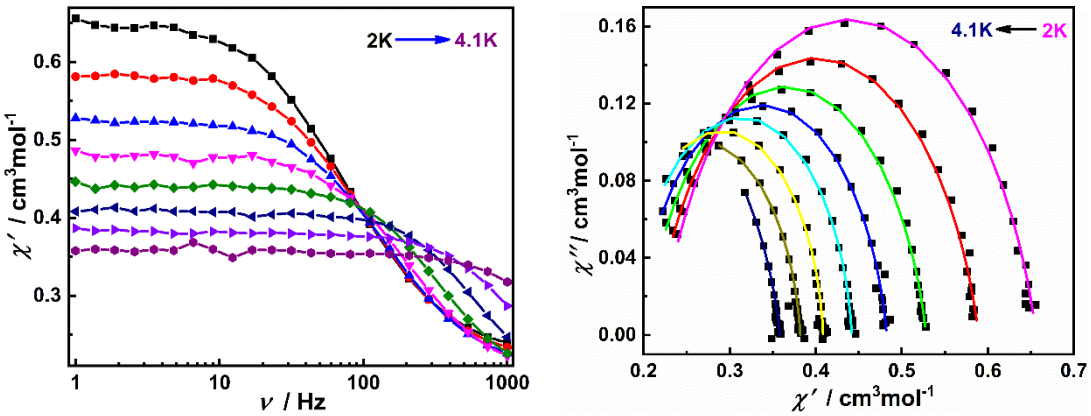


**Fig. S12** Frequency dependence of in-phase (left) ac susceptibility data under a 2000 Oe dc field for **L-2**. Cole–Cole plots for **L-2** (right). The solid lines are the best fits to a generalized Debye model.

**Table S6** Cole-Cole parameters of **L-2** at a 2000 Oe dc field.

| $T$ / K | $\chi_S$ / cm$^{-3}$mol$^{-1}$ | $\chi_T$ / cm$^{-3}$mol$^{-1}$ | $\tau$ / s | $\alpha$ | R |
|---|---|---|---|---|---|
| 2 | 2.19E-01 | 6.56E-01 | 1.99E-03 | 1.81E-01 | 3.64E-04 |
| 2.3 | 2.12E-01 | 5.89E-01 | 1.51E-03 | 1.71E-01 | 5.71E-04 |
| 2.6 | 2.02E-01 | 5.28E-01 | 1.09E-03 | 1.49E-01 | 1.83E-04 |
| 2.9 | 1.92E-01 | 4.82E-01 | 7.47E-04 | 1.24E-01 | 3.88E-04 |
| 3.2 | 1.85E-01 | 4.42E-01 | 4.60E-04 | 8.23E-02 | 1.57E-04 |
| 3.5 | 1.73E-01 | 4.09E-01 | 2.57E-04 | 6.60E-02 | 1.32E-04 |
| 3.8 | 1.52E-01 | 3.82E-01 | 1.27E-04 | 8.71E-02 | 9.32E-05 |
| 4.1 | 4.19E-02 | 3.58E-01 | 3.65E-05 | 1.52E-01 | 4.44E-04 |

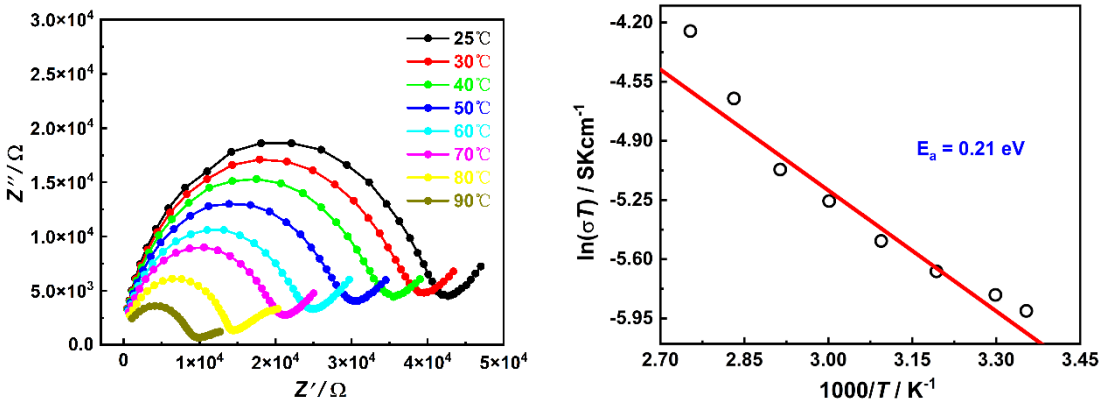


**Fig. S13** Nyquist plots of **D-1** at different temperatures under 98% relative humidity (left). The ln($\sigma T$) versus 1000/$T$ curve of **D-1** (right). The red solid lines are the best fit using the Arrhenius law.

**Table S7** The proton conductivity of **D-1, L-1** and **L-2** at 98% relative humidity under variable temperature (°C).

| Temperature / °C | σ / S cm$^{-1}$（**D-1**） | σ / S cm$^{-1}$（**L-1**） | σ / S cm$^{-1}$（**L-2**） |
|---|---|---|---|
| 25 | 9.13E-6 | 4.39E-6 | 2.71E-6 |
| 30 | 9.87E-6 | 5.15E-6 | 2.88E-6 |
| 40 | 1.09E-5 | 6.43E-6 | 3.53E-6 |
| 50 | 1.27E-5 | 8.36E-6 | 4.32E-6 |
| 60 | 1.56E-5 | 1.17E-5 | 5.01E-6 |
| 70 | 1.83E-5 | 1.50E-5 | 7.13E-6 |
| 80 | 2.70E-5 | 2.20E-5 | 9.09E-6 |
| 90 | 3.92E-5 | 3.20E-5 | 1.30E-5 |

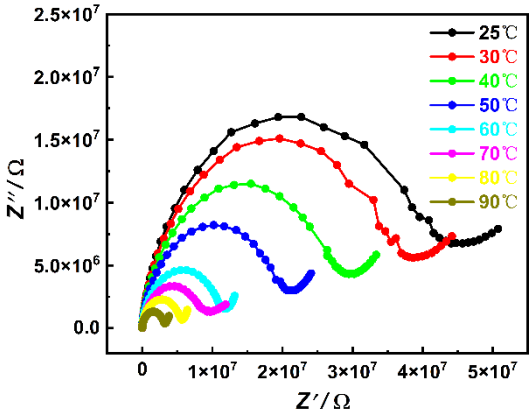


**Fig. S14** Nyquist plots of **D-1** at different temperatures under 75% relative humidity

**Table S8** The proton conductivity of **D-1** at 75% relative humidity under variable temperature (°C).

| Temperature / °C | σ / S cm$^{-1}$（**D-1**） |
|---|---|
| 25 | 7.66E-9 |
| 30 | 8.73E-9 |
| 40 | 1.11E-8 |
| 50 | 1.59E-8 |
| 60 | 2.81E-8 |
| 70 | 3.47E-8 |
| 80 | 5.98E-8 |
| 90 | 1.05E-7 |